


RESEARCH ARTICLE

Electronically Controlled Broadband Terahertz Amplitude Modulator Based on Ionic Liquid/PEDOT:PSS:DMSO Composite Structure

Yangqi Liu¹ , Bo Zhang¹  and Yan Zhang^{1,*} 

¹Department of Physics, Capital Normal University, China

Abstract: Electronically controlled modulation devices operating in the terahertz (THz) band offer a crucial foundation for the integration and minimization of THz systems. In this work, we offer a broadband THz amplitude modulator that can be electrically controlled. The modulator is based on a composite structure made of ionic liquid and polymer mixture poly (3-ethoxythiophenyl): poly (4-phenylsulfonate) (PEDOT:PSS:DMSO). By applying merely +4 V excitation and −4 V turn-off voltage, a 40% amplitude modulation depth may be produced in the frequency region of 0.1–1.5 THz due to the joint action of electrons in the polymer and ions in the ionic liquid. The measurement of the resistance change of the polymer surface provides an explanation and confirmation of the mechanism of polymer action in this occurrence. This work provides a material selection for a simple preparation, inexpensive, and effective modulation of THz amplitude for an ionic liquid gate electronically controlled THz modulator. It is also expected that this work can be helpful for the miniaturization and integration development of THz modulators.

Keywords: terahertz, electric control, ionic liquid, PEDOT:PSS, modulator

1. Introduction

Terahertz (THz) radiations affect a wide range of fields, including security detection, medical imaging, molecular biology, and next-generation communication systems [1–5]. Functional devices such as filters [6], polarizers [7, 8], and modulators [9–14] are essential for speeding up applications related to spectroscopy, imaging, and communication. THz modulators are essential parts of high-speed data transfer, high-resolution imaging systems, and THz wireless communications. Broadband performance, low transient, and low energy cost are essential for THz modulators. Numerous publications on the development of THz modulators based on diverse materials have been published. The public's anxiety over electronically controlled THz modulators stems from their versatility and universality. An electric-controlled dual-band modulator on n-GaAs with a unique patterned metallic structure was proposed by Min et al. [15]. Two distinct split strips that would resonate at two different frequency bands (0.58 THz and 1.0 THz) made up the metamaterial structure cell. A modulator that used a DC bias voltage to dynamically adjust the alignment of liquid crystal (LC) molecules was proposed by Yang et al. [16]. The electro-optic characteristics of LC and devices at various DC biases are examined using a THz time-domain spectroscopy. In the particular operational frequency region, resonance shifting, tunable electromagnetically induced transparency, and electromagnetically induced absorption have all been seen under various DC bias directions and polarization directions of incident THz waves. The

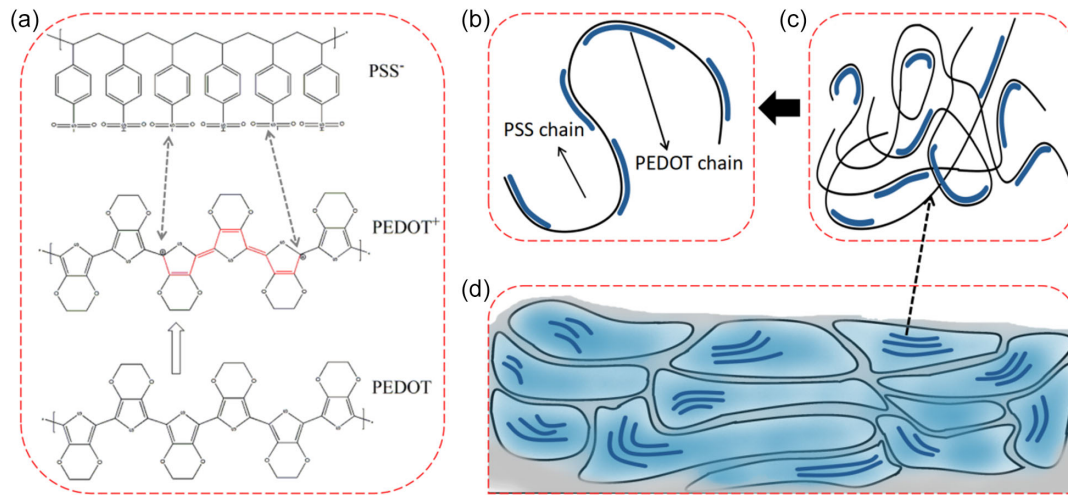
aforementioned articles make clear that the majority of known electronically controlled THz modulators employ a combination of semiconductor materials. Traditional electronic control circuits face difficulties in generating and accumulating carriers. Nevertheless, achieving the previously specified structural functions is challenging for semiconductor materials that can work in the THz region. Therefore, to enable electrically controlled carrier creation and stacking, a new approach is required.

Ionic liquid-based (IL) graphene gating devices have attracted a lot of research interest recently. Wu et al. [17] showed off the greater performance of THz modulators built on a sandwich architecture of IL and graphene in 2015. By applying a gate voltage of 3 V, the modulation covers a broadband frequency range from 0.1 to 2.5 THz with a modulation depth of up to 99% [17]. di Gaspare et al. [18] presented a gate-tunable single layer graphene that operated in the 1–5 THz range. The graphene was implanted in a quarter-wave cavity. 40% optical amplitude modulation depth is guaranteed by the employment of an electrolyte IL gate. The performance of ion liquid gate electronic control modulators using graphene thin films as functional layers is excellent. However, graphene thin-film materials are relatively expensive and the preparation process is quite complex. It is valuable to find some semiconductor films that can replace graphene films as functional layers in ion liquid gate electronic modulators. In 2021, Karst et al. [19] reported an electrically switchable metal polymer nanoantenna that can switch between conductor and insulator states by applying excitation voltages of +1 V and −1 V under the action of a conductive ion solution. The properties of conductive particle solutions are similar to those of ILs, indicating the potential of PEDOT:PSS to form modulators with IL gates.

*Corresponding author: Yan Zhang, Department of Physics, Capital Normal University, China. Email: yzhang@cnu.edu.cn

Figure 1

- (a) Chemical structure of PEDOT:PSS. The commonly described microstructure of conducting polymer system,
 (b) PEDOT:PSS is synthesized on the long chain of PSS, (c) colloidal gel particles are formed in the dispersion, and (d) thin films containing PEDOT (blue) and PSS (gray)



Meanwhile, the price of PEDOT:PSS is cheaper and the method of preparing thin films is simple, which meets the research expectations.

Polymer mixture poly (3-ethoxythiophenyl): poly (4-phenylsulfonate) (PEDOT:PSS) has excellent thermal stability, high transparency, carrier mobility, and conductivity. Figure 1(a) depicts its chemical composition. The PEDOT oligomer is thought to have polymerized onto the long chain of PSS (Figure 1(b)), indicating that PEDOT possesses intrinsic flaws in its relative molecular weight and polydispersity. A polyanion (PSS) rich shell (Figure 1(c)), which aids in stabilizing PEDOT rich particles in aqueous solution, is typically found in the gel-like particles that make up the PEDOT:PSS dispersion [20]. P-stacking is evident in Figure 1(d), which depicts gel particles that have been formed in a pancake-like structure [21–23]. Chemical doping with ethylene glycol and dimethyl sulfoxide (DMSO) can be used to customize its electrical conductivity [24–27]. A material made up of free ions in liquid form at or close to room temperature is referred to as an IL. Anion and cation are joined by the Coulomb force in ionic compounds. Certain ionic compounds have a high anion and cation volume and a loose structure, which results in little force between the ions and a melting point that is near ambient temperature. Due to their unique ionic transport characteristics and conductivity, ILs have garnered a lot of attention and are utilized in a variety of applications, including high-performance batteries and solar cells [28–30]. A flexible multilayer graphene infrared device based on porous polyethylene film was disclosed [31]. IL intercalation allows for the adjustment of the infrared emissivity in this device. The infrared emissivity of surface graphene is changed from 0.57 to 0.41 following the intercalation of IL. Surface graphene's relative reflectance rose from 1.0 to 1.15 during the same period. Kee et al. [32] stated in 2020 that by altering the IL additive, it is possible to adjust the mechanical and electrical properties of the representative CP-PEDOT:PSS. PEDOT:PSS conductivity was greatly increased by the cationic/anionic alteration of IL, reaching up to 1075 S/cm. The high conductivity PEDOT:PSS:IL film also exhibited good mechanical and electrical tensile capabilities, allowing it to retain its initial conductivity under 80% strain [32]. These studies have demonstrated the electrical sensitivity and modifiable features of IL and semiconductor hybrid structures, which has piqued our intense

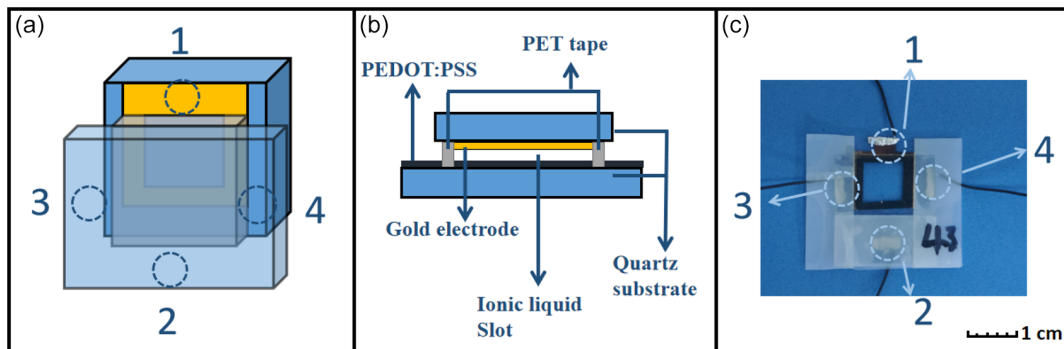
curiosity. Development of THz electronic dynamic devices is anticipated to be possible, thanks to the semiconductor and IL hybrid structure's electrical sensitivity and adjustable features.

In this work, a method for controlling charge carriers in semiconductor materials using ion-containing electrical circuits was studied. The ions can be driven near and away from the PEDOT:PSS:DMSO film by applying an electric field to the IL, thereby achieving the dynamic control of the THz transmission. The amplitude modulation depth can reach 40% by applying a high voltage of +4 V and a low voltage of −4 V, and the modulation speed is 7 Hz. A relatively uniform modulation can be achieved in the range of 0.1–1.5 THz. The experimental mechanism of device's electrical excitation was explained, and the proposed experimental mechanism was verified using the R (resistance)-T (measurement time) curve. This work provides a cheaper, simpler, and effective material selection for the electrically controlled THz modulator based on IL gate. At the same time, it is also expected that this work can be helpful for the miniaturization and integration development of THz modulators.

2. Experiment and Method

With the chemical CAS number 143314-16-3, EMIM-BF₄, also known as 1-Ethyl-3-methylimidazolium tetrafluoroborate, is the IL that was used in this work. It is frequently employed as a reaction medium because it is a superior electrolyte. The techniques of spin coating and heat evaporation were used to create the three-layer structure samples. A quartz sheet measuring 25 mm in length, 25 mm in width, and 1 mm in thickness was spun using a 9:1 weight ratio solution of PEDOT:PSS and DMSO. The quartz sheet was then dried at 100 °C for 15 min, with the PEDOT:PSS film having a thickness of about 30 nm [33]. Next, as illustrated in Figure 2(a), the quartz sheet covered with PEDOT:PSS:DMSO film was adhered to a quartz sheet that had been plated with gold electrodes. In this manner, a 100 μm-thick vacant slot appears between two quartz slices. Using a syringe, the EMIM-BF₄ was injected into the vacant slot until the liquid level was flush with the slot's aperture. To enhance the visual representation of the sample structure, Figure 2(b) presents

Figure 2
Structure diagram of the sample (a) side view and (b) top view. (c) Optical image of the sample (Electrodes 1 and 2 are used to apply excitation voltage, while Electrodes 3 and 4 are employed for measuring thin-film resistance)



a top view of the sample structure. Figure 2(c) displays an optical image of the sample following wire bonding. Electrodes 1 and 2 are responsible for excitation voltage, while Electrodes 3 and 4 are employed for measuring thin-film resistance. A homemade THz time-domain spectroscopy is employed to measure the THz spectra [34]. The femtosecond light beam generated by an amplifier has an average power of 900 mW, the repetition ratio is 1 kHz, the center wavelength of 800 nm, and the pulse width of 50 fs. THz waves were radiated and detected using ZnTe crystals. A translation platform is moved during the test to alter the relative optical path difference between the THz pulses and probe beam. This allows the point-by-point scanning of the entire THz time-domain spectrum with a step of and the step size is 0.01 mm. The THz spot has a diameter of 1 mm.

An electrical testing system is used to confirm the modulation mechanism during the electronically controlled dynamic modulation of the sample. A digital source meter, a computer, and an excitation power supply make up the system. The DC and AC power supplies needed for testing are provided by the digital source meter. The sample's voltage and current are measured and fed into a computer. The sample receives an excitation voltage from the power supply.

3. Experimental Results

The samples are tested using a homemade THz time-domain spectroscopy. The time-domain spectra of a sample at various bias voltages are displayed in Figure 3(a). The THz signal peak value increases from 0.8 to 1 in comparison to the case of no bias voltage when 1 V, 2 V, 3 V, and 4 V voltages are applied on the PEDOT:PSS:DMSO/EMIM-BF₄/electrode sample. It can be seen that the peak values obtained at the application of 1 V, 2 V, 3 V, and 4 V excitation voltages are the same. It decreases to 0.6 when a -4 V voltage is applied. Based on these observations, it can be concluded that the amplitude modulation depth can reach 40% with a small bias voltage of ± 4 V. The response speed and the film's capacity to tolerate instantaneous current during positive and negative voltage switching are the primary factors that went into choosing 4 V. (The higher the voltage, the faster the response speed, but high voltage can easily damage the PEDOT:PSS:DMSO film). Figure 3(b) displays the frequency domain THz spectra of a sample with varying bias voltages. The virtually identical shapes of the spectra show that the device can regulate the THz radiation's amplitude uniformly over a large range. In order to clearly demonstrate the working bandwidth of the sample,

the experimental results were normalized based on the frequency domain spectral intensity with 4 V excitation voltage. Figure 3(c) shows the transmittance of the sample at different frequencies with different excitation voltages. The device's ability to consistently accomplish about 40% amplitude modulation in the 0.1–1.5 THz frequency range indicates that it is a wide-band modulator. To confirm that PEDOT:PSS:DMSO thin film is the cause of this phenomena, an Electrode/EMIM-BF₄/Electrode sample control experiment was also carried out. Figure 3(d) shows that there is no discernible difference in the time-domain spectra whether the excitation voltages are applied or not. This means that the device without the PEDOT:PSS:DMSO layer does not have the ability to electrically modulate THz wave.

The peak change diagram of square wave voltage switching is used to quantify the sample's response speed to an electrical stimulus. By measuring the peak variation of the time-domain spectrum during a switch with a ± 4 V square wave voltage, one may determine how quickly the sample responds to electrical excitation. As can be observed from Figure 4(a), the sample's THz transmittance increases from 0.6 to 1 in 60 ms when a +4 V excitation voltage is supplied (as indicated by the yellow area). The sample's THz transmittance drops from 1 to 0.6 in 80 ms when a -4 V excitation voltage is supplied, as seen in Figure 4(b) (yellow area). This allows for the calculation of the sample's response speed for the square wave excitation voltage, which comes out to be about 7 Hz. When a 4 V excitation voltage is applied (rising edge), the resistance of PEDOT:PSS film increases, and the ions move fast, so the transmittance of the THz wave increases quickly. However, when a -4 V excitation voltage is applied (falling edge), the film resistance decreases, and the ion movement speed is slow. This results that the time of the rising edge is shorter than that of the falling edge. The transmission speed of ILs and the current-withstanding capacity of PEDOT:PSS:DMSO thin films are the primary factors limiting the device response speed.

The flow of electrons from the gold electrode toward the PEDOT:PSS film and their binding to the holes in the film are diagrammed in Figure 5(a), where a +4 V voltage is supplied for excitation (the long arrow in the figure denotes the direction of travel of electrons and ions). The blue region in Figure 5(a) illustrates this process. At the same time, the BF₄⁻ ions travel toward the gold electrode and the EMIM⁺ ions move toward the PEDOT:PSS:DMSO layer. Through this method, the conductivity of the PEDOT:PSS thin film is decreased together with the number of holes in them increases; thus, the device exhibits a

Figure 3

- (a) THz time-domain spectra of reference and PEDOT:PSS:DMSO/EMIM-BF₄/electrode sample with different bias voltage, (b) THz spectrum of reference and PEDOT:PSS:DMSO/EMIM-BF₄/electrode samples with different bias voltages, (c) Transmission of PEDOT:PSS:DMSO/EMIM-BF₄/electrode samples with the excitation voltage at different frequencies, and (d) spectra of electrode/EMIM-BF₄/electrode sample with different bias voltages

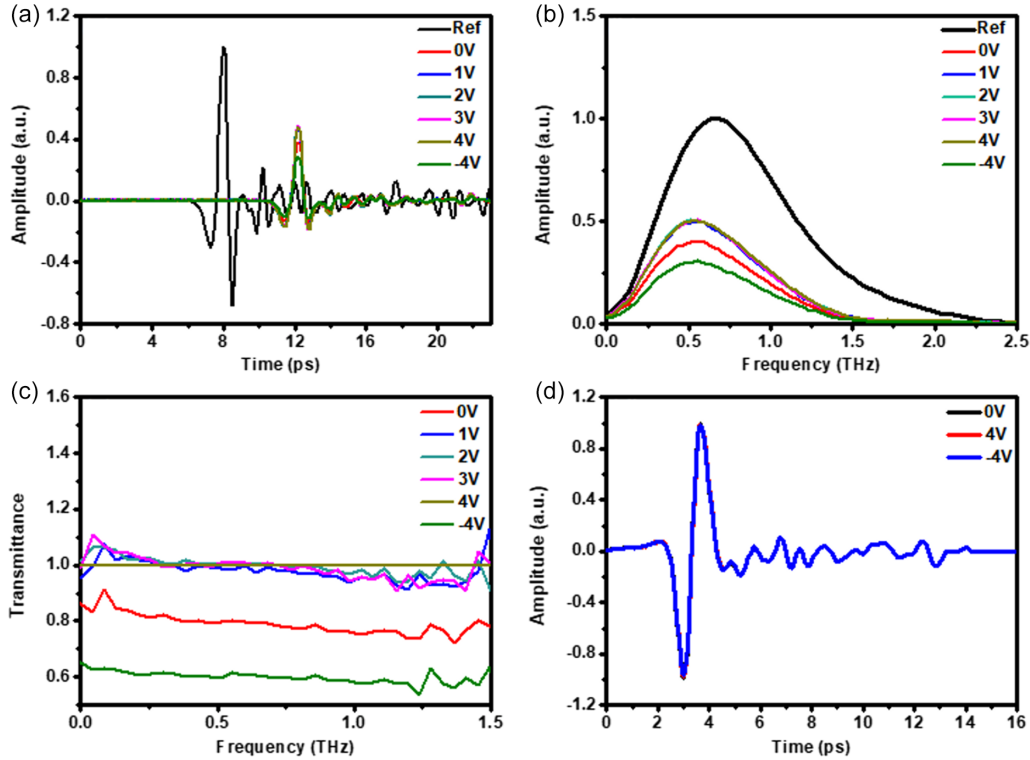
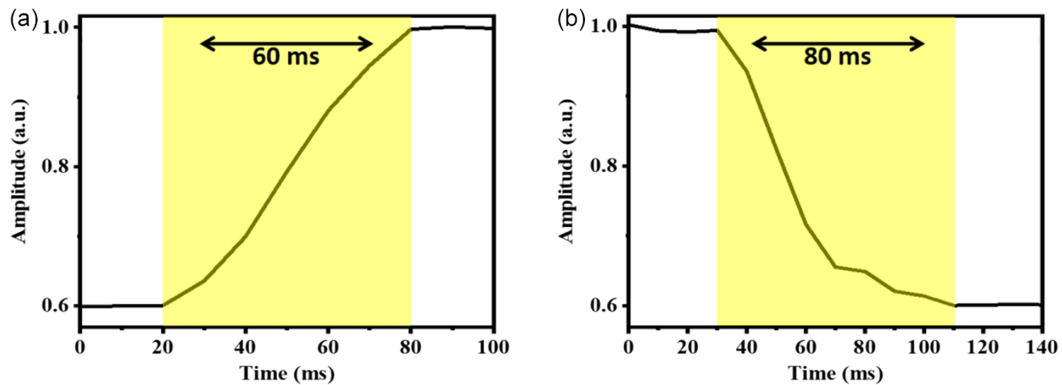


Figure 4

- (a) Rising edge of the sample's response to +4 V excitation voltage and (b) falling edge of the sample's response to -4 V excitation voltage



stronger THz wave transmission. On the other hand, as illustrated in Figure 5(b), when a voltage of -4 V is applied, holes are released in the PEDOT:PSS film and electrons go from the film to the gold electrode. Simultaneously, EMIM⁺ ions travel toward the gold electrode while BF₄⁻ ions in the IL move toward the PEDOT:PSS:DMSO layer. By doing this, the PEDOT:PSS film returns to its original condition of conductivity. The device shows a low THz wave transmission at this time [35].

According to the aforementioned main rationale, the device's variation in THz transmission is caused by a change in PEDOT:

PSS thin-film conductivity. The resistance change of the film in the high and low potential variations was evaluated to support this mechanism. The sample is initially excited at low voltage (blue line) and has 410 Ω of resistance, as can be seen in Figure 6. The resistance increases to 18000 Ω when the high voltage (red line) is switched on. As the voltage changes to low voltage, the film resistance goes back to 410 Ω . Get the same outcomes by repeating this procedure multiple times. This outcome is consistent with the experimental procedure described above. Figure 6 illustrates how the conductivity properties of ILs cause

Figure 5
Working principle of the device at an excitation voltage of (a) +4 V and (b) -4 V

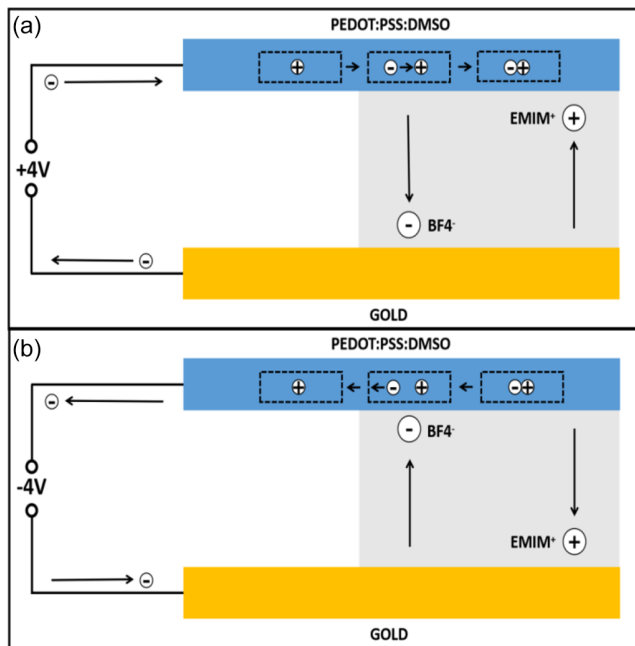
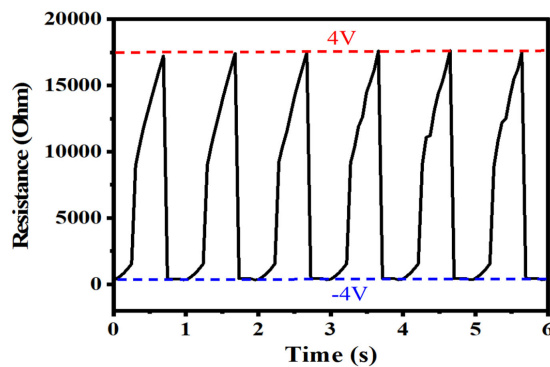


Figure 6
Resistance of PEDOT:PSS:DMSO film at high and low voltage



the transmittance to increase quickly after providing a +4 V excitation voltage, then slowly thereafter. When the excitation voltage is applied, the concentration of moving ions in the IL will increase; thus, the ion transport capacity is strong. The holes in the film can join with the electrons and the resistance of the film increases quickly. As the time for applied excitation voltage increases, the concentration of flowing ions in the IL will fall, and then the ion transport capacity drops; thus, the electron acquisition speed drops also. Therefore, the growth of film's resistance slows down. The device just presents a moderate modulation depth and frequency, the performance can be improved through better electrode design, thinner IL layers, and lower loss substrates. The advantage of this device is low cost and easy fabrication.

4. Conclusion

Finally, we provide a broadband THz amplitude modulator that can be electrically controlled, based on the IL/PEDOT:PSS:DMSO

composite structure. With the application of +4 V and -4 V excitation and shutdown voltage to regulate the mobility of electrons in polymers and ions in IL, it can achieve 40% amplitude modulation of THz signal in the frequency range of 0.1–1.5 THz. The modulation speed is 7 Hz. The flow of ions and electrons within the apparatus under varying voltage excitations provides the experimental explanation of this phenomena. The thin film's capacity to transport holes is altered by electron mobility, which modifies the film resistance. This work provides a material selection for a simple preparation, inexpensive, and effective modulation of THz amplitude for an IL gate electronically controlled THz modulator. We also hope to promote the miniaturization and integration development of THz functional devices.

Funding Support

This work was supported by the National Natural Science Foundation of China [Grant Nos. 11774246 and 121774271] and the Sino-German Mobility Program of the Sino-German Center for Science Funding (Grant No. M-0225).

Ethical Statement

This study does not contain any studies with human or animal subjects performed by any of the authors.

Conflicts of Interest

Yan Zhang is an editorial board member for *Journal of Optics and Photonics Research* and was not involved in the editorial review or the decision to publish this article. The authors declare that they have no conflicts of interest to this work.

Data Availability Statement

Data are available from the corresponding author upon reasonable request.

Author Contribution Statement

Yangqi Liu: Conceptualization, Investigation, Writing – original draft, Writing – review & editing, Visualization. **Bo Zhang:** Investigation, Resources, Funding acquisition. **Yan Zhang:** Conceptualization, Writing – review & editing, Project administration, Funding acquisition.

References

- [1] Fu, X., Liu, Y., Chen, Q., Fu, Y., & Cui, T. J. (2022). Applications of terahertz spectroscopy in the detection and recognition of substances. *Frontiers in Physics*, 10, 869537. <https://doi.org/10.3389/fphy.2022.869537>
- [2] Bai, S., & Yang, H. (2022). New proposals for application of terahertz imaging technique in Chinese medicine. *Chinese Journal of Integrative Medicine*, 28(4), 366–373. <https://doi.org/10.1007/s11655-022-2886-3>
- [3] Wang, P., Lou, J., Fang, G., & Chang, C. (2022). Progress on cutting-edge infrared-terahertz biophysics. *IEEE Transactions on Microwave Theory and Techniques*, 70(11), 5117–5140. <https://doi.org/10.1109/TMTT.2022.3200333>
- [4] Li, L., Ge, H., Jiang, Y., Li, G., Lv, M., Wang, F., & Zhang, Y. (2022). Tài hệt bô zài 6G tōngxìn wǎngluò zhōng de yánjiū jìnzhǎn [Research progress of terahertz waves in 6G communication networks]. *Laser & Optoelectronics*

- Progress*, 59(13), 1300007. <https://doi.org/10.3788/LOP202259.1300007>
- [5] He, Y., & Ma, C. (2022). Analysis of the effect of antenna pointing error caused by satellite perturbation on space terahertz communication. *Applied Sciences*, 12(21), 10772. <https://doi.org/10.3390/app122110772>
 - [6] Lv, X., Ako, R. T., Bhaskaran, M., Sriram, S., Fumeaux, C., & Withayachumnankul, W. (2022). Frequency-selective-surface-based mechanically reconfigurable terahertz bandpass filter. *IEEE Transactions on Terahertz Science and Technology*, 12(3), 257–266. <https://doi.org/10.1109/TTHZ.2022.3148816>
 - [7] Li, J., Yue, Z., Li, J., Zheng, C., Liu, J., Yang, F., . . . , & Yao, J. (2023). Bō qián kě kòng guī quán tài hēzī chāo jiégòu qǐ piān qì [Wavefront-controllable all-silicon terahertz meta-polarizer]. *Science China Materials*, 66(1), 300–308. <https://doi.org/10.1007/s40843-022-2126-0>
 - [8] Bundel, P., Wu, G. B., Chen, B. J., & Chan, C. H. (2023). Wideband circular polarizer for a photoconductive antenna. *Optics Letters*, 48(12), 3223–3226. <https://doi.org/10.1364/OL.488037>
 - [9] Su, H., Zheng, Z., Yu, Z., Feng, S., Lan, H., Wang, S., . . . , & Liang, H. (2023). Optically controlling broadband terahertz modulator based on layer-dependent PtSe₂ nanofilms. *Nanomaterials*, 13(5), 795. <https://doi.org/10.3390/nano13050795>
 - [10] Gong, S., Ping, D., Bi, C., Zhang, Z., Liang, S., Wang, L., . . . , & Zhang, Y. (2022). High-performance direct terahertz modulator based on resonance mode transformation for high-speed wireless communication. *Applied Physics Letters*, 121(23), 231104. <https://doi.org/10.1063/5.0121712>
 - [11] Gou, H. G., Zhu, Y., Wu, Z. D., Shi, G. H., & Lai, W. E. (2023). Jīyú yīn/tàn nànmǐ kēlǐ jīn hóngwài qū dòng de dà tiáo zhì shēn dù tài hēzī tiáo zhì qì [NIR-driven large modulation depth terahertz modulator based on silver/carbon nanoparticles]. *Journal of Infrared and Millimeter Waves*, 42(4), 476–482. <https://doi.org/10.11972/j.issn.1001-9014.2023.04.008>
 - [12] Tao, S. N., Shen, Z. X., Yu, H. G., Wang, H. C., Ge, S. J., & Hu, W. (2022). Transflective spatial terahertz wave modulator. *Optics Letters*, 47(7), 1650–1653. <https://doi.org/10.1364/OL.450764>
 - [13] Zhang, P., Cai, T., Zhou, Q., She, G., Liang, W., Deng, Y., . . . , & Zhang, C. (2022). Ultrahigh modulation enhancement in all-optical Si-based THz modulators integrated with gold nanobipyramids. *Nano Letters*, 22(4), 1541–1548. <https://doi.org/10.1021/acs.nanolett.1c04229>
 - [14] Wang, S., Su, M., Tang, L., Li, X., Li, X., Bai, H., . . . , & Yao, J. (2023). Graphene-coated D-shaped terahertz fiber modulator. *Frontiers in Physics*, 11, 1202839. <https://doi.org/10.3389/fphy.2023.1202839>
 - [15] Min, W., Sun, H., Zhang, Q., Ding, H., Shen, W., & Sun, X. (2016). A novel dual-band terahertz metamaterial modulator. *Journal of Optics*, 18(6), 065103. <https://doi.org/10.1088/2040-8978/18/6/065103>
 - [16] Yang, L., Fan, F., Chen, M., Zhang, X., & Chang, S. J. (2017). Active terahertz metamaterials based on liquid-crystal induced transparency and absorption. *Optics Communications*, 382, 42–48. <https://doi.org/10.1016/j.optcom.2016.07.055>
 - [17] Wu, Y., La-o-vorakiat, C., Qiu, X., Liu, J., Deorani, P., Banerjee, K., . . . , & Yang, H. (2015). Graphene terahertz modulators by ionic liquid gating. *Advanced Materials*, 27(11), 1874–1879. <https://doi.org/10.1002/adma.201405251>
 - [18] di Gaspare, A., Pogna, E. A. A., Riccardi, E., Sarfraz, S. M. A., Scamarcio, G., & Vitiello, M. S. (2022). All in one-chip, electrolyte-gated graphene amplitude modulator, saturable absorber mirror and metrological frequency-tuner in the 2–5 THz range. *Advanced Optical Materials*, 10(22), 2200819. <https://doi.org/10.1002/adom.202200819>
 - [19] Karst, J., Floess, M., Ubl, M., Dingler, C., Malacrida, C., Steinle, T., . . . , & Giessen, H. (2021). Electrically switchable metallic polymer nanoantennas. *Science*, 374(6567), 612–616. <https://doi.org/10.1126/science.abj3433>
 - [20] Zhou, H., Chua, M. H., Zhu, Q., & Xu, J. (2021). High-performance PEDOT:PSS-based thermoelectric composites. *Composites Communications*, 27, 100877. <https://doi.org/10.1016/j.coco.2021.100877>
 - [21] Lang, U., Müller, E., Naujoks, N., & Dual, J. (2009). Microscopical investigations of PEDOT:PSS thin films. *Advanced Functional Materials*, 19(8), 1215–1220. <https://doi.org/10.1002/adfm.200801258>
 - [22] Nardes, A. M., Kemerink, M., Janssen, R. A. J., Bastiaansen, J. A. M., Kiggen, N. M. M., Langeveld, B. M. W., . . . , & de Kok, M. M. (2007). Microscopic understanding of the anisotropic conductivity of PEDOT:PSS thin films. *Advanced Materials*, 19(9), 1196–1200. <https://doi.org/10.1002/adma.200602575>
 - [23] Takano, T., Masunaga, H., Fujiwara, A., Okuzaki, H., & Sasaki, T. (2012). PEDOT nanocrystal in highly conductive PEDOT:PSS polymer films. *Macromolecules*, 45(9), 3859–3865. <https://doi.org/10.1021/ma300120g>
 - [24] Wang, W., Ji, H., Liu, D., Xiong, L., Hou, Y., Zhang, B., & Shen, J. (2018). Active bidirectional electrically-controlled terahertz device based on dimethyl sulfoxide-doped PEDOT:PSS. *Optics Express*, 26(20), 25849–25857. <https://doi.org/10.1364/OE.26.025849>
 - [25] Xu, Y., Liu, Z., Wei, X., Wu, J., Guo, J., Zhao, B., . . . , & Dou, Y. (2021). Morphological modulation to improve thermoelectric performances of PEDOT:PSS films by DMSO vapor post-treatment. *Synthetic Metals*, 271, 116628. <https://doi.org/10.1016/j.synthmet.2020.116628>
 - [26] Lingstedt, L. V., Ghittorelli, M., Lu, H., Koutsouras, D. A., Marszalek, T., Torricelli, F., . . . , & Blom, P. W. M. (2019). Effect of DMSO solvent treatments on the performance of PEDOT:PSS based organic electrochemical transistors. *Advanced Electronic Materials*, 5(3), 1800804. <https://doi.org/10.1002/aelm.201800804>
 - [27] Yan, F., Parrott, E. P. J., Ung, B. S. Y., & Pickwell-MacPherson, E. (2015). Solvent doping of PEDOT:PSS: Effect on terahertz optoelectronic properties and utilization in terahertz devices. *The Journal of Physical Chemistry C*, 119(12), 6813–6818. <https://doi.org/10.1021/acs.jpcc.5b00465>
 - [28] Wolny, A., & Chrobok, A. (2022). Silica-based supported ionic liquid-like phases as heterogeneous catalysts. *Molecules*, 27(18), 5900. <https://doi.org/10.3390/molecules27185900>
 - [29] Zhang, Y., Qiao, X., Zhao, W., Sun, J., Tang, Q., Du, Y., . . . , & Ji, Q. (2020). Highly sensitive gas-sensing films for volatile organic acids from imidazolium-based Poly(ionic liquid)s. *Journal of Nanoscience and Nanotechnology*, 20(6), 3588–3597. <https://doi.org/10.1166/jnn.2020.17403>
 - [30] Ma, P., Fang, Y., Li, A., Wen, B., Cheng, H., Zhou, X., . . . , & Lin, Y. (2021). Highly efficient and stable ionic liquid-based

- gel electrolytes. *Nanoscale*, 13(15), 7140–7151. <https://doi.org/10.1039/D0NR08765C>
- [31] Zhao, L., Zhang, R., Deng, C., Peng, Y., & Jiang, T. (2019). Tunable infrared emissivity in multilayer graphene by ionic liquid intercalation. *Nanomaterials*, 9(8), 1096. <https://doi.org/10.3390/nano9081096>
- [32] Kee, S., Kim, N., Park, H., Kim, B. S., Teo, M. Y., Lee, S., ..., & Lee, K. (2020). Tuning the mechanical and electrical properties of stretchable PEDOT:PSS/ionic liquid conductors. *Macromolecular Chemistry and Physics*, 221(23), 2000291. <https://doi.org/10.1002/macp.202000291>
- [33] Liu, J., Liu, B., Liu, D., Xiong, L., Shen, J., & Zhang, B. (2020). Active bidirectionally controlled terahertz interference fringe shift in DMSO-doped PEDOT:PSS film. *Applied Physics Letters*, 117(4), 043301. <https://doi.org/10.1063/5.0011845>
- [34] Ji, H., Zhang, B., Wang, W., Lv, L., & Shen, J. (2018). Ultraviolet light-induced terahertz modulation of an indium oxide film. *Optics Express*, 26(6), 7204–7210. <https://doi.org/10.1364/OE.26.007204>
- [35] Machrafi, H., Bobinac, I., Dongo, P., Gallo, V., Iermano, F., & Iorio, C. S. (2021). Chemical stability and reversibility of PEDOT:PSS electrodes in view of low-cost biocompatible cellulose-assisted biosensors. *Materials Today Communications*, 27, 102437. <https://doi.org/10.1016/j.mtcomm.2021.102437>

How to Cite: Liu, Y., Zhang, B., & Zhang, Y. (2024). Electronically Controlled Broadband Terahertz Amplitude Modulator Based on Ionic Liquid/PEDOT:PSS:DMSO Composite Structure. *Journal of Optics and Photonics Research*. <https://doi.org/10.47852/bonviewJOPR42022788>